Task-Space Modular Dynamics for Dual-Arms Expressed through a Relative Jacobian

Rodrigo S. Jamisola Jr.[1], Petar S. Kormushev[2], Rodney G. Roberts[3], Darwin G. Caldwell[4]

[1]*Department of Electrical, Computer and Telecommunications Engineering*
Botswana International University of Science and Technology, Palapye, Botswana

[2] *Dyson School of Design Engineering, Imperial College London, U.K.*

[3]*Department of Electrical and Computer Engineering*
Florida State University, Tallahassee, Florida, U.S.A.

[4]*Department of Advanced Robotics*
Istituto Italiano di Tecnologia, Via Morego, 30 16163 Genova, Italy

Abstract

This paper presents modular dynamics for dual-arms, expressed in terms of the kinematics and dynamics of each of the stand-alone manipulators. The two arms are controlled as a single manipulator in the task space that is relative to the two end-effectors of the dual-arm robot. A modular relative Jacobian, derived from a previous work, is used which is expressed in terms of the stand-alone manipulator Jacobians. The task space inertia is expressed in terms of the Jacobians and dynamics of each of the stand-alone manipulators. When manipulators are combined and controlled as a single manipulator, as in the case of dual-arms, our proposed approach will not require an entirely new dynamics model for the resulting combined manipulator. But one will use the existing Jacobians and dynamics model for each of the stand-alone manipulators to come up with the dynamics model of the combined manipulator. A dual-arm KUKA is used in the experimental implementation.

Keywords: Modular dynamics, modular relative Jacobian, dual-arms, combined manipulators, dual-arm KUKA, chain-cleaning task, wrench transformation matrix

Email address: jamisolar@biust.ac.bw, p.kormushev@imperial.ac.uk, rroberts@fsu.edu, darwin.caldwell}@iit.it (Rodrigo S. Jamisola Jr.[1], Petar S. Kormushev[2], Rodney G. Roberts[3], Darwin G. Caldwell[4])

1. Introduction

Nowadays, robots become much more complicated compared to their single-arm, stand-alone manipulator predecessor. And because of the need for them to interact more with humans, robots take on biological forms like humans themselves, e.g., dual-arms and humanoids, and in many cases like animals, e.g., dog-, cheetah-, gecko-, spider-, snake-robots, etc. In most cases, these robots in biological forms are combined manipulators. That is, they are created by combining two or more stand-alone manipulators in parallel or series connection or both. Normally, their degrees of freedom (DOFs) are much higher. For dual-arms (as shown in Fig. 1) and humanoids, the DOFs are: 25 for Compliant Humanoid (CoMan) [1], 34 for Honda Asimo's P2 [2], 41 for iCub upper body [3], 43 for DLR's dual-arm [4], and 51 for mobile humanoid Rollin' Justin [5], to name a few.

It is well-known that for complex robots interacting with their environments, the dynamics model provides an optimal controller in real-time [6]. For combined manipulators, their much more complex structures necessitate a dynamics model in order to simulate their physical behavior and subsequently gain a much better understanding of their physical characteristics. This is crucial in the design of their appropriate controllers [7]. Thus, until at the very recent, the dynamics model of combined manipulators is still actively studied. For humanoids, these studies include the effects in modelling and simulating a human or a humanoid [8], task and whole body motion coordination with active force control [9], a dynamics simulator for humanoid robots [10, 11], dynamic balance force control for determining full body joint torques [12, 13], sequential optimization for impact motions of humanoid robots [14], human-humanoid postures with external disturbances [15], centroidal dynamics of humanoids [16], humanoid complete dynamics [17], and decoupled dynamics for NASA-JSC Valkyrie [18]. For dual-arm robots, studies on their dynamics model include dynamics of a flexible dual-arm robot using Lagrange formulation [19], modular dynamics with inertias expressed at the joint-space level [20], dynamics of a dual-arm space robot [21, 22], dynamics of a dual-arm robot for load transport under sliding mode control [23, 24], dynamics with elasticity at the joints [25], and dynamics of rigid dual-arms carrying a flexible load [26].

However for combined manipulators, their complete dynamics formulation can be prohibitively complicated. One way to address this complexity is to simplify the dynamics model by modularizing it. That is, we use the existing dynamics model of each of the stand-alone manipulators and combine them together to form the dynamics model of the entire system. In this way, one will not need to derive an entirely new dynamics expression because the existing dynamics expression from the stand-alone manipulators can still be utilized. To formulate the modular dynamics of combined manipulators, we need to consider two fundamental types of connections: parallel (dual-arm) and series (macro-mini) connections.

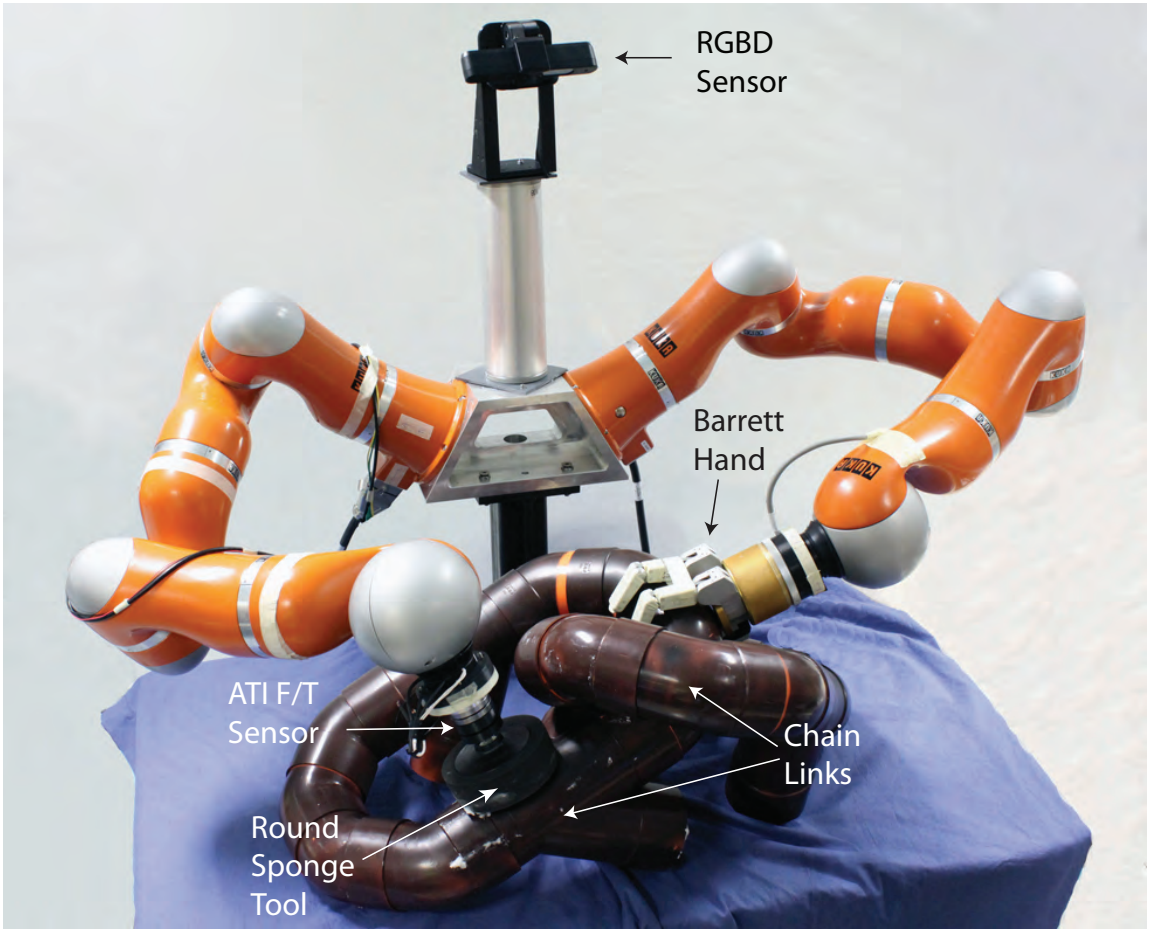

Figure 1: A KUKA dual-arm setup in a chain-cleaning task. The left hand is equipped with a gripper tool (Barrett hand), while the right hand (with a force/torque sensor) is attached with a sponge cleaning tool. A vision module determines the location for gripping and cleaning.

This paper aims to derive the modular dynamics formulation of a parallel-connected combined manipulator, a dual-arm, controlled as a single manipulator with single end-effector. The treatment of a dual-arm as a single end-effector manipulator through the use of the relative Jacobian [27–29] affords a drastic increase in the null-space dimension and lesser constraints in the task space. It considers the relative motion between the end-effectors such that one end-effector (tool end-effector) moves relative to another end-effector (reference end-effector). The relative motion of the tool end-effector with respect to the reference end-effector is considered to be the single end-effector motion for the dual-arm. Absolute motion can be imposed on the reference end-effector. This work ex-

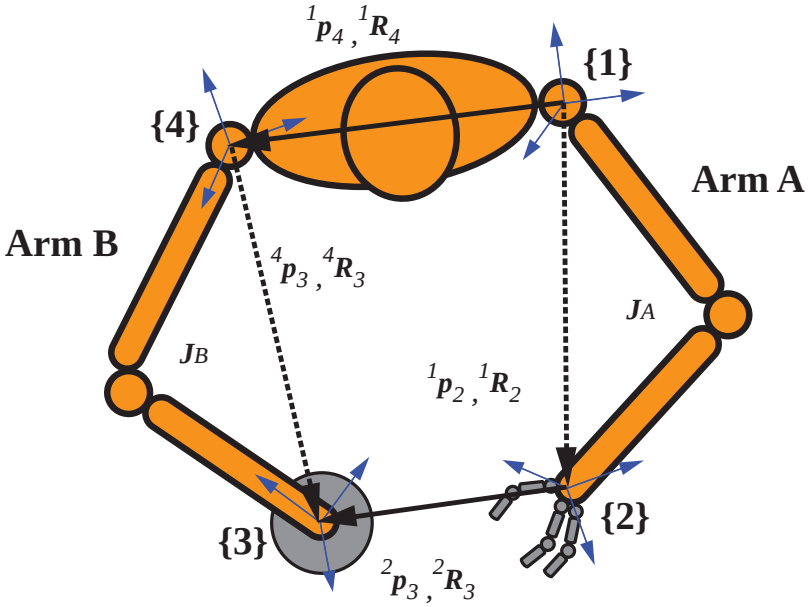

Figure 2: An schematic of the dual-arm setup. Arm A (reference arm) is attached with a gripper, and Arm B (tool arm) is attached with a cleaning tool. Corresponding positions and orientations with respect to the attached reference frames {1}, {2}, {3}, and {4} are shown.

tends the use of modular relative Jacobian for dual arms [29] by incorporating the modular dynamics into the kinematics model.

2. The Relative Jacobian

A modular relative Jacobian is shown in [29] and is stated here for convenience. First let us consider the dual-arm setup shown in Fig. 1 where the left (reference) arm grips a chain model, while the right (tool) arm cleans the chain model with a sponge tool. Its corresponding frame assignment is shown in Fig. 2. Given the stand-alone Jacobian of the reference robot (arm A), $\mathbf{J}_A$, and the stand-alone Jacobian of the tool robot (arm B), $\mathbf{J}_B$, the modular relative Jacobian, $\mathbf{J}_R$, expressed with respect to the frame assignment shown in Fig. 2 can be expressed as

$$\mathbf{J}_R = \begin{bmatrix} \mathbf{Q}_A \mathbf{J}_A & \mathbf{Q}_B \mathbf{J}_B \end{bmatrix} \tag{1}$$

where

$$\mathbf{Q}_A = -\begin{bmatrix} \mathbf{I} & -S(^2\mathbf{p}_3) \\ \mathbf{0} & \mathbf{I} \end{bmatrix} \begin{bmatrix} ^2\mathbf{R}_1 & \mathbf{0} \\ \mathbf{0} & ^2\mathbf{R}_1 \end{bmatrix} \quad \text{and} \quad \mathbf{Q}_B = \begin{bmatrix} ^2\mathbf{R}_4 & \mathbf{0} \\ \mathbf{0} & ^2\mathbf{R}_4 \end{bmatrix} \tag{2}$$

such that position vector ${}^{i}\mathbf{p}_j$, and rotation matrix ${}^{i}\mathbf{R}_j$ are expressed with respect to the reference frames $\{i\}$ and $\{j\}$. A wrench transformation matrix ${}^{2}\Psi_3$ is defined as

$$ {}^{2}\Psi_3 = \begin{bmatrix} \mathbf{I} & -S({}^{2}\mathbf{p}_3) \\ \mathbf{0} & \mathbf{I} \end{bmatrix}. \tag{3} $$

The symbol $S({}^{2}\mathbf{p}_3)$ is a skew symmetric matrix with vector input ${}^{2}\mathbf{p}_3$ defined as

$$ {}^{2}\mathbf{p}_3 = {}^{2}\mathbf{R}_1 \; {}^{1}\mathbf{p}_4 + {}^{2}\mathbf{R}_4 \; {}^{4}\mathbf{p}_3 - {}^{2}\mathbf{R}_1 \; {}^{1}\mathbf{p}_2. \tag{4} $$

The relative task-space velocity for the dual-arm, $\dot{\mathbf{x}}_R$, can be expressed as

$$ \dot{\mathbf{x}}_R = \mathbf{Q}_A \, \dot{\mathbf{x}}_A + \mathbf{Q}_B \, \dot{\mathbf{x}}_B \tag{5} $$

where $\dot{\mathbf{x}}_A$ and $\dot{\mathbf{x}}_B$ are the task-space velocities of robots A and B, respectively.

3. Modular Dynamics in the Relative Task Space

In this section, we present the modular dynamics of the dual-arm robot in the relative task space. Let us assign $\mathbf{x}_R$ to be the relative position and orientation between the end-effectors, that is, the end-effector of robot B (tool robot) with respect to the end-effector of robot A (reference robot), as shown in Fig. 2. The rest of the conventions used for both robots A and B, respectively, are: joint space displacements, $\mathbf{q}_A$ and $\mathbf{q}_B$; joint space inertias, $\mathbf{A}_A$ and $\mathbf{A}_B$; joint torques, τ_A and τ_B; Coriolis and centrifugal forces, $\mathbf{h}_A$ and $\mathbf{h}_B$; and gravitational terms, $\mathbf{g}_A$ and $\mathbf{g}_B$. A dot or double dot on top of a parameter means its corresponding first or second derivative, respectively. Given the full dynamics expression of robot A to be $\tau_A = \mathbf{A}_A \, \ddot{\mathbf{q}}_A + \mathbf{h}_A + \mathbf{g}_A$ and the full dynamics expression of robot B to be $\tau_B = \mathbf{A}_B \, \ddot{\mathbf{q}}_B + \mathbf{h}_B + \mathbf{g}_B$, the modular dynamics in the relative task space for the dual-arm robot, formulated based on the operational space formulation [6, 30] but expressed on terms of the relative Jacobian, can be stated as

$$ \tau_T = \mathbf{J}_R^T \, \Lambda_R \, \ddot{\mathbf{x}}_R + (\mathbf{I} - \mathbf{J}_R^T \mathbf{J}_R^{\#T}) \, \tau_o - \mathbf{J}_R^{+} \, \Lambda_R \, \dot{\mathbf{J}}_R \, \dot{\mathbf{q}}_T + \mathbf{h}_T + \mathbf{g}_T \tag{6} $$

where $\tau_T = [\tau_A^T \; \tau_B^T]^T$, $\dot{\mathbf{q}}_T = [\dot{\mathbf{q}}_A^T \; \dot{\mathbf{q}}_B^T]^T$, $\mathbf{h}_T = [\mathbf{h}_A^T \; \mathbf{h}_B^T]^T$, $\mathbf{g}_T = [\mathbf{g}_A^T \; \mathbf{g}_B^T]^T$, and τ_o is the torque gradient in the null space. Thus, the modular relative task space inertia, Λ_R, is given as

$$ \Lambda_R = \mathbf{Q}_A^{-1} \, \mathbf{J}_A^{+T} \, \mathbf{A}_A \, \mathbf{J}_A^{+} \, \mathbf{Q}_A^{-1} + \mathbf{Q}_B^{-1} \, \mathbf{J}_B^{+T} \, \mathbf{A}_B \, \mathbf{J}_B^{+} \, \mathbf{Q}_B^{-1}. \tag{7} $$

The superscript "T" means transpose, superscript "+" means pseudoinverse, and superscript "-1" means inverse. The relative Jacobian, $\mathbf{J}_R$, is shown in (1); $\mathbf{Q}_A$ and $\mathbf{Q}_B$ are

defined in (2); $\mathbf{J}_A$ and $\mathbf{J}_A$ are standalone Jacobians of robots A and B; and, $\mathbf{A}_A$ and $\mathbf{A}_B$ are the standalone joint inertias of robots A and B.

The dynamically consistent inverse [6] is defined as

$$\mathbf{J}_R^{\#T} = \Lambda_R \Big[\mathbf{Q}_A \, \mathbf{J}_A \, \mathbf{A}_A^{-1} \quad \mathbf{Q}_B \, \mathbf{J}_B \, \mathbf{A}_B^{-1} \Big]. \tag{8}$$

The expression in (6) has a similar form as the standard full dynamics expression for a single, stand-alone manipulator. Thus the full dynamics expression of the dual-arm now becomes analogous to the full dynamics of a single end-effector manipulator. This affords a single manipulator control for the dual-arm. Another advantage of this approach is its modularity: we use the kinematics and dynamics model of each of the stand-alone manipulators to arrive at the full dynamics expression of the dual-arm. Through this approach, we do not require to derive a totally new dynamics expression for the dual-arm, but we make use of existing model of the stand-alone manipulators to come up with the full dynamics model of the dual-arm.

The next section will shows the derivation of (7) which will imply (8). A non-modular approach is shown in Appendix A.

4. Derivation of Modular Inertia for Dual-Arm

In this section, we derive the total inertia for dual-arm robot in terms of the joint space and relative task space. The total joint-space inertia for the dual-arm is labelled $\mathbf{A}_T$, and the relative task-space inertia of the dual-arm is labelled $\mathbf{\Lambda}_T$.

The total joint space kinetic energy of the dual-arm robot, KE_T, can be expressed as

$$KE_T = \frac{1}{2} \, \dot{\mathbf{q}}_T^T \, \mathbf{A}_T \, \dot{\mathbf{q}}_T \tag{9}$$

where $\dot{\mathbf{q}}_T = [\dot{\mathbf{q}}_A^T \; \dot{\mathbf{q}}_B^T]^T$ is the combined joint angles.

The joint space kinetic energy of robot A, KE_{JA}, and the joint space kinetic energy of robot B, KE_{JB}, can be expressed as

$$KE_{JA} = \frac{1}{2} \, \dot{\mathbf{q}}_A^T \, \mathbf{A}_A \, \dot{\mathbf{q}}_A \quad \text{and} \quad KE_{JB} = \frac{1}{2} \, \dot{\mathbf{q}}_B^T \, \mathbf{A}_B \, \dot{\mathbf{q}}_B. \tag{10}$$

Because both joint space kinetic energies are independent of each other, the total joint space kinetic energy can be added as $KE_T = KE_{JA} + KE_{JB}$, that is

$$\begin{aligned} KE_T &= \frac{1}{2} \, \dot{\mathbf{q}}_A^T \, \mathbf{A}_A \, \dot{\mathbf{q}}_A + \frac{1}{2} \, \dot{\mathbf{q}}_B^T \, \mathbf{A}_B \, \dot{\mathbf{q}}_B \\ &= \frac{1}{2} \begin{bmatrix} \dot{\mathbf{q}}_A^T & \dot{\mathbf{q}}_B^T \end{bmatrix} \begin{bmatrix} \mathbf{A}_A & \mathbf{0} \\ \mathbf{0} & \mathbf{A}_B \end{bmatrix} \begin{bmatrix} \dot{\mathbf{q}}_A \\ \dot{\mathbf{q}}_B \end{bmatrix} \\ &= \frac{1}{2} \, \dot{\mathbf{q}}_T^T \begin{bmatrix} \mathbf{A}_A & \mathbf{0} \\ \mathbf{0} & \mathbf{A}_B \end{bmatrix} \dot{\mathbf{q}}_T \end{aligned} \tag{11}$$

Comparing the above equation to (9), this means that

$$\mathbf{A}_T = \begin{bmatrix} \mathbf{A}_A & \mathbf{0} \\ \mathbf{0} & \mathbf{A}_B \end{bmatrix}. \tag{12}$$

Now, we consider the total task-space kinetic energy for the dual-arm, KE_O, stated below

$$KE_O = \frac{1}{2}\, \dot{\mathbf{x}}_R^T\, \mathbf{\Lambda}_R\, \dot{\mathbf{x}}_R. \tag{13}$$

We use the general relationship between task-space inertia $\mathbf{\Lambda}$, joint-space inertia $\mathbf{A}$, and Jacobian $\mathbf{J}$ from [30], that is, $\mathbf{\Lambda} = [\mathbf{J}\mathbf{A}^{-1}\,\mathbf{J}^T]^+$. Because robot A moves independent of robot B, its task-space kinetic energy, KE_{SA}, is

$$\begin{aligned} KE_{SA} &= \frac{1}{2}\, \dot{\mathbf{x}}_R^T \left[\begin{bmatrix} \mathbf{Q}_A\, \mathbf{J}_A & \mathbf{0} \end{bmatrix} \begin{bmatrix} \mathbf{A}_A^{-1} & \mathbf{0} \\ \mathbf{0} & \mathbf{0} \end{bmatrix} \begin{bmatrix} \mathbf{J}_A^T\, \mathbf{Q}_A^T \\ \mathbf{0}^T \end{bmatrix} \right]^+ \dot{\mathbf{x}}_R \\ &= \frac{1}{2}\, \dot{\mathbf{x}}_R^T \left[\mathbf{Q}_A\, \mathbf{J}_A\, \mathbf{A}_A^{-1}\, \mathbf{J}_A^T\, \mathbf{Q}_A^T \right]^+ \dot{\mathbf{x}}_R \\ &= \frac{1}{2}\, \dot{\mathbf{x}}_R^T\, \mathbf{Q}_A^{-T}\, \mathbf{J}_A^{+T}\, \mathbf{A}_A\, \mathbf{J}_A^+\, \mathbf{Q}_A^{-1}\, \dot{\mathbf{x}}_R. \end{aligned} \tag{14}$$

In the same way, robot B moves independent of robot A, thus its task-space kinetic energy, KE_{SB}, is

$$\begin{aligned} KE_{SB} &= \frac{1}{2}\, \dot{\mathbf{x}}_R^T \left[\begin{bmatrix} \mathbf{0} & \mathbf{Q}_B\, \mathbf{J}_B \end{bmatrix} \begin{bmatrix} \mathbf{0} & \mathbf{0} \\ \mathbf{0} & \mathbf{A}_B^{-1} \end{bmatrix} \begin{bmatrix} \mathbf{0}^T \\ \mathbf{J}_B^T\, \mathbf{Q}_B^T \end{bmatrix} \right]^+ \dot{\mathbf{x}}_R \\ &= \frac{1}{2}\, \dot{\mathbf{x}}_R^T \left[\mathbf{Q}_B\, \mathbf{J}_B\, \mathbf{A}_B^{-1}\, \mathbf{J}_B^T\, \mathbf{Q}_B^T \right]^+ \dot{\mathbf{x}}_R \\ &= \frac{1}{2}\, \dot{\mathbf{x}}_R^T\, \mathbf{Q}_B^{-T}\, \mathbf{J}_B^{+T}\, \mathbf{A}_B\, \mathbf{J}_B^+\, \mathbf{Q}_B^{-1}\, \dot{\mathbf{x}}_R. \end{aligned} \tag{15}$$

Thus, the total task-space kinetic energy of dual-arms is $KE_O = KE_{SA} + KE_{SB}$,

$$KE_O = \frac{1}{2}\, \dot{\mathbf{x}}_R^T \left[\mathbf{Q}_A^{-T}\, \mathbf{J}_A^{+T}\, \mathbf{A}_A\, \mathbf{J}_A^+\, \mathbf{Q}_A^{-1} + \mathbf{Q}_B^{-T}\, \mathbf{J}_B^{+T}\, \mathbf{A}_B\, \mathbf{J}_B^+\, \mathbf{Q}_B^{-1} \right] \dot{\mathbf{x}}_R, \tag{16}$$

which means that the modular task-space inertia of a dual-arm, $\mathbf{\Lambda}_R$, is

$$\Lambda_R = \mathbf{Q}_A^{-T}\, \mathbf{J}_A^{+T}\, \mathbf{A}_A\, \mathbf{J}_A^+\, \mathbf{Q}_A^{-1} + \mathbf{Q}_B^{-T}\, \mathbf{J}_B^{+T}\, \mathbf{A}_B\, \mathbf{J}_B^+\, \mathbf{Q}_B^{-1}. \tag{17}$$

5. Dual-Arm Experimental Implementation

We present two sets of experiments using our proposed method. First is a chain-cleaning task that shows uninterrupted relative chain-cleaning motion of the tool end-effector, despite real-time displacement of the absolute location of the reference (gripper) end-effector. Second is an investigative experiment on the effect of the wrench transformation matrix to the relative Jacobian.

5.1. Gravity Compensation

The default gravity compensation setting for the KUKA lightweight arm is for the horizontal floor mounting where gravity vector $\mathbf{g} = [0, 0, -9.81]^T$. In order to correct the 60 degrees inclination of the torso mounting (and another 30 degrees rotation around the resulting z-axis), the following gravity compensation corrections were performed: for the right arm

$$\mathbf{g}_r = \mathbf{R}_{z,30}\, \mathbf{R}_{y,-60}\, \mathbf{g} \tag{18}$$

and the left arm

$$\mathbf{g}_l = \mathbf{R}_{z,-30}\, \mathbf{R}_{y,-60}\, \mathbf{g} \tag{19}$$

where $\mathbf{R}_{a,b}$ is the rotation matrix for a corresponding rotation along the a-axis for b-degree angle. This results into $\mathbf{g}_r = [-7.36, -4.25, 4.91]^T$ and $\mathbf{g}_l = [-7.36, 4.25, 4.91]^T$.

5.2. Relative Jacobian Transformations

Here we define the transformation matrices $\mathbf{Q}_A$ and $\mathbf{Q}_B$ shown in (2) of the modular relative Jacobian. These transformations are characterized on how the bases of robots A and B are placed with respect to each other.

The rotation matrix ${}^2\mathbf{R}_1$ corresponds to the rotation of the left hand (robot A) end-effector with respect to its base, $\mathbf{R}_A$. The rotation matrix ${}^2\mathbf{R}_4 = {}^2\mathbf{R}_1\, {}^1\mathbf{R}_4 = \mathbf{R}_A\, {}^1\mathbf{R}_4$ such that

$${}^1\mathbf{R}_4 = \mathbf{R}_{z,-30}\, \mathbf{R}_{y,-120}\, \mathbf{R}_{z,150}. \tag{20}$$

The relative position vector between the end-effectors of the two arms shown in (4) can be expressed as

$${}^2\mathbf{p}_3 = \mathbf{R}_A^T\, {}^1\mathbf{p}_4 + \mathbf{R}_A^T\, {}^1\mathbf{R}_4\, \mathbf{p}_B - \mathbf{R}_A^T\, \mathbf{p}_A \tag{21}$$

where vectors $\mathbf{p}_A$ and $\mathbf{p}_B$ are the robots A and B end-effector positions with respect to their corresponding bases. Such that

$${}^1\mathbf{p}_4 = \mathbf{R}_{z,-30}\, \mathbf{R}_{y,-150}\, {}^1\mathbf{p}_{4\_base} \tag{22}$$

where ${}^1\mathbf{p}_{4\_base} = [0, 0, 0.22]^T m$.

5.3. Relative Hybrid Force/Position Controller

This work does not claim contribution on hybrid force/position controller. However, we present the integration of the controller here for clarity of presentation in the control implementation.

From (6), $\ddot{\mathbf{x}}_R$ can be replaced by the controller $\mathbf{u}_R^*$ such that

$$\mathbf{u}_R^* = \Omega_R\, \mathbf{f}_P^* \;+\; \bar{\Omega}_R\, \mathbf{f}_F^* \tag{23}$$

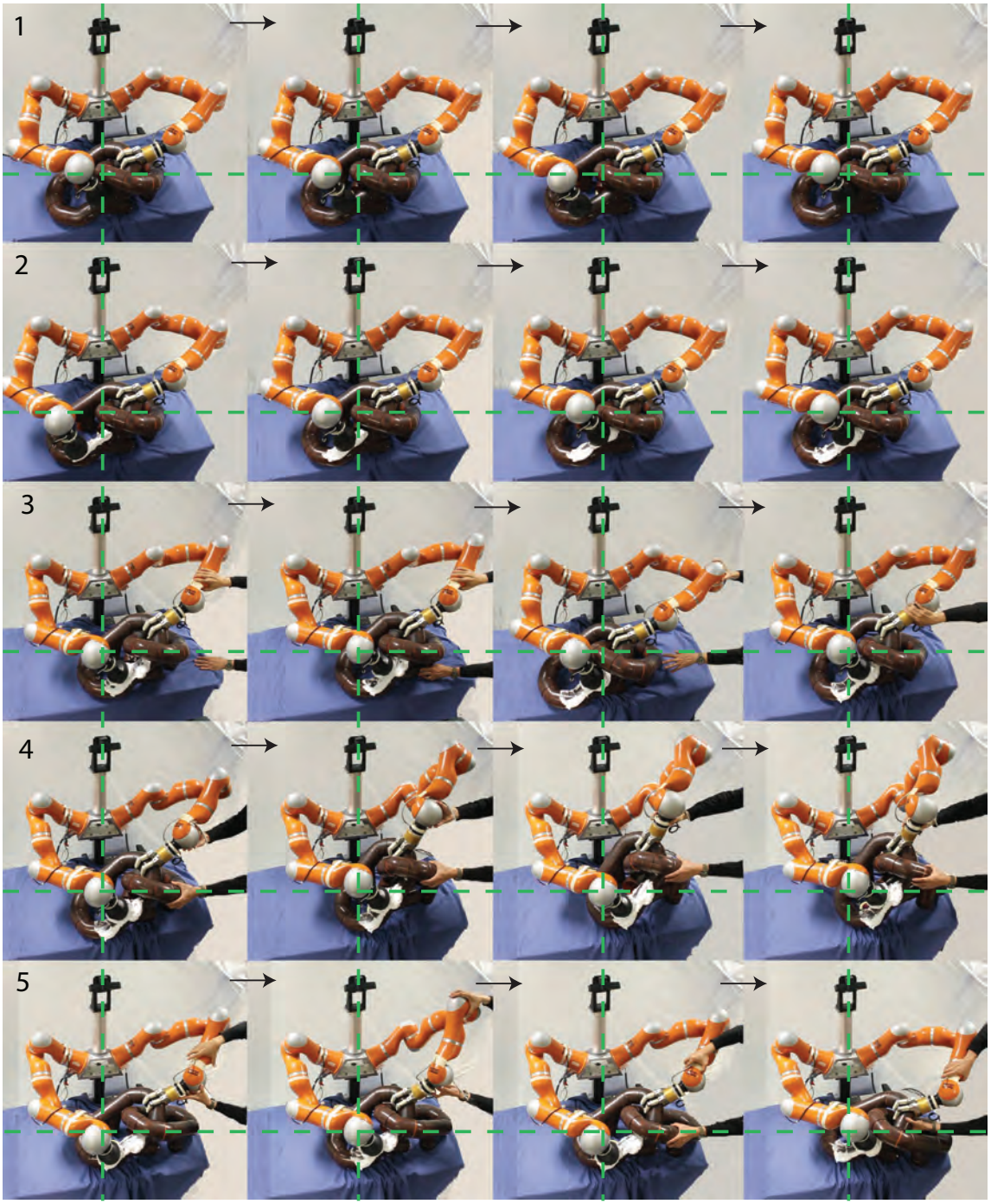

Figure 3: Snapshots of the chain-cleaning task. Horizontal strip 1 shows the cleaning task where the location of the tool and the gripper are manually placed. Horizontal strip 2 shows the same cleaning task where the shaving foam is used to assign the chain portion for cleaning and gripping. In horizontal strip 3, disturbance is introduced to the gripper arm by moving the gripper horizontally along the table. In horizontal strip 4, the gripper is moved vertically during task execution. And lastly, horizontal strip 5 shows vertical and horizontal disturbance to the gripper arm, as well as null space posture disturbance.

where $\mathbf{f}_P^*$ is the relative position (and orientation) controller, $\mathbf{f}_F^*$ is the relative force (and moment) controller, and Ω_R and $\bar{\Omega}_R$ are the corresponding selection matrices where one is the complement of the other. For simplicity, we refer to the relative position and orientation controller as relative position controller, and relative force and moment controller as relative force controller.

Thus the relative position controller can be expressed as

$$\mathbf{f}_P^* = \ddot{\mathbf{x}}_{R_d} - \mathbf{k}_{v_P}(\dot{\mathbf{x}}_R - \dot{\mathbf{x}}_{R_d}) - \mathbf{k}_{p_P}(\mathbf{x}_R - \mathbf{x}_{R_d}) \tag{24}$$

where $\ddot{\mathbf{x}}_{R_d}, \dot{\mathbf{x}}_{R_d}, \mathbf{x}_{R_d}$ are the desired relative task space acceleration, velocity, and displacement, respectively, and parameters $\mathbf{k}_{p_P}$ and $\mathbf{k}_{v_P}$ are the proportional and derivative gains for position control. The relative force controller can be expressed as

$$\mathbf{f}_F^* = \mathbf{f}_{R_d} - \mathbf{k}_{p_F}(\mathbf{f}_R - \mathbf{f}_{R_d}) - \int_0^t \mathbf{k}_{i_F}(\mathbf{f}_R - \mathbf{f}_{R_d})\, dt \tag{25}$$

where $\mathbf{f}_{R_d}$ is the desired relative applied force, $\mathbf{f}_R$ is the relative force feedback, parameters $\mathbf{k}_{p_F}$ and $\mathbf{k}_{i_F}$ are the relative proportional and integral force control gains, and t is time. The relative selection matrices can be expressed as follows

$$\Omega_R = \begin{pmatrix} \mathbf{R}_R^T \Sigma_R \mathbf{R}_R & \mathbf{0} \\ \mathbf{0} & \mathbf{R}_R^T \Sigma_R \mathbf{R}_R \end{pmatrix} \tag{26}$$

and

$$\bar{\Omega}_R = \begin{pmatrix} \mathbf{R}_R^T \bar{\Sigma}_R \mathbf{R}_R & \mathbf{0} \\ \mathbf{0} & \mathbf{R}_R^T \bar{\Sigma}_R \mathbf{R}_R \end{pmatrix} \tag{27}$$

where Σ_R is a diagonal matrix with diagonal elements of zeros and ones which specifies the desired axes of position control, $\bar{\Sigma}_R$ is the complement of Σ_R that specifies the axes of force control where position is not controlled, and $\mathbf{R}_R$ is the corresponding rotation matrix that specifies the direction of the independent axes for force or position control.

5.4. Experiment 1: Chain-Cleaning Task

We implement a hybrid force/position control in a chain-cleaning task, that has a similar force and motion controller as the aircraft canopy polishing task [31, 32], where its dynamics modeling and identification are shown in [33–35]. The purpose of the experiment is to show how the task coordination between the two end-effectors remain uninterrupted, as the absolute task location is arbitrarily changed in real-time. In this earlier implementation of our controller, only the position and force are controlled. Orientation and moment are not controlled and thus their corresponding controller gains are set to zero.

For all vectors, the subscripts for the position components are x, y, and z and for the orientation components are α, β, and γ. For example, $\mathbf{x}_R = [x_{R_x}, x_{R_y}, x_{R_z}, x_{R_\alpha}, x_{R_\beta}, x_{R_\gamma}]^T$. From (23), position is controlled along x_{R_x}- and x_{R_z}-axes, while force is controlled along the x_{R_y}-axis. Such that the selection matrices have the following diagonal terms $\text{diag}(\Omega_R) = \{1,0,1,0,0,0\}$ and $\text{diag}(\bar{\Omega}_R) = \{0,1,0,0,0,0\}$. Now we set the values of proportional gains for position and force. From (24), we set $\mathbf{k}_{p_P} = [100,0,100,0,0,0]^T$ such that the desired position along x_{R_x}-axis is the initial position. The desired position along the x_{R_z}-axis is set to a sinusoidal path $x_{R_{dz}} = A\sin(\omega t)$, where $A = 0.12\ m$ and $\omega = 1.26\ rad/s$. From (25), we set $\mathbf{k}_{p_F} = [0,0.2,0,0,0,0]^T$ such that the desired force along the y-axis is set at $f_{R_{dy}} = 10\ N$. The $\mathbf{k}_{p_P}$ values are chosen such that non-zero values are set in the directions that are position controlled, i.e., along the $x-$ and $z-$ axes. And $\mathbf{k}_{p_F}$ values are chosen such that non-zero value is set in the direction that is force controlled, i.e., along the $y-$axis. The gains were empirically chosen such that the end-effectors remains stable at the fastest response. Given the controller information above, and the joint space inertia and gravity terms for both robots A and B, the task space formulation in (6) is implemented for a dual-arm KUKA consisting of two LWR robots. Information regarding Coriolis and centrifugal terms were not available during the experiments. No null-space controller is implemented thus the torque τ_o is set to zero.

Snapshots during the chain-cleaning task are shown in Fig. 3. Each horizontal photo strip shows one case of the chain-cleaning task. Horizontal photo strip 1 shows the cleaning task where the location of the gripper and the cleaning tool are manually set. That is, the operator manually moves the end-effectors to the locations for gripping and cleaning, then manually attaches the gripper on the chain and manually places the cleaning tool at its starting cleaning location. Horizontal photo strip 2 shows the same task where a shaving foam is used to specify location on the chain for cleaning or gripping, as detected by the RGBD sensor. The RGBD sensor is calibrated to identify the location of the shaving foam: one location for gripping and another for cleaning. At the start of the task, each end-effector will approach their respective desired locations based on the RGBD sensor feedback. When the end-effector settles to their desired locations, the operator then manually attaches the gripper and adjusts the cleaning tool to position. The robot response is shown in Fig. 4, with the relative positions x_{R_x} and x_{R_z}, the relative force f_{R_y}, and the absolute positions of the gripper (reference) end-effector x_{A_x}, x_{A_y}, and x_{A_z} which remain stationary.

In the succeeding experiments, the same case applies as in horizontal photo strip 2: the desired gripping and cleaning locations of the dual-arm end-effectors are determined by the RGBD sensor feedback. Moreover, disturbances are introduced by the operator by manually moving the dual-arm end-effectors, in real-time, as the chain-cleaning task is performed. In horizontal photo strip 3, the chain is dragged together with the reference

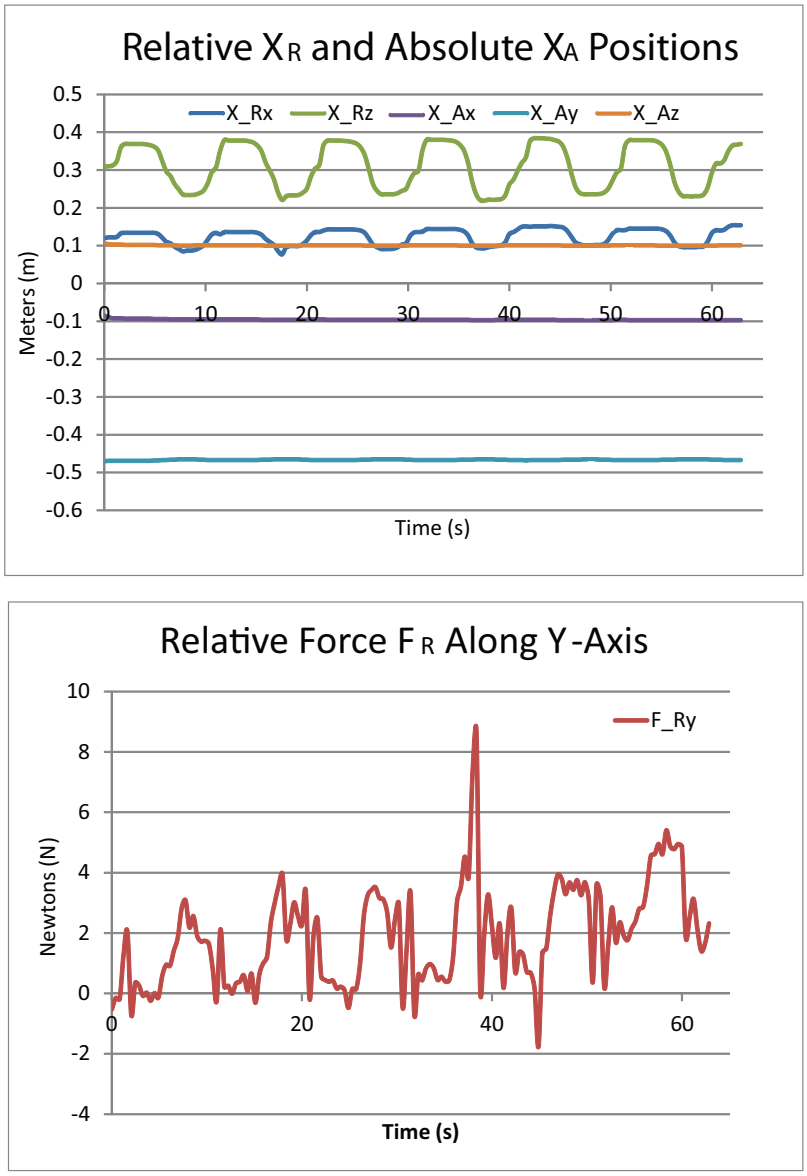

Figure 4: The graphs show the relative position along x_{R_x} and x_{R_z} and relative force f_{Ry} during the chain cleaning task. The absolute position and orientation of the gripper (reference) end-effector, $\mathbf{x}_A$, is arbitrary and not moving.

end-effector on the table surface. As shown in the horizontal strip the tool end-effector responded automatically to achieve the desired relative position and force with respect to the reference end-effector. In horizontal photo strip 4, the reference end-effector is moved

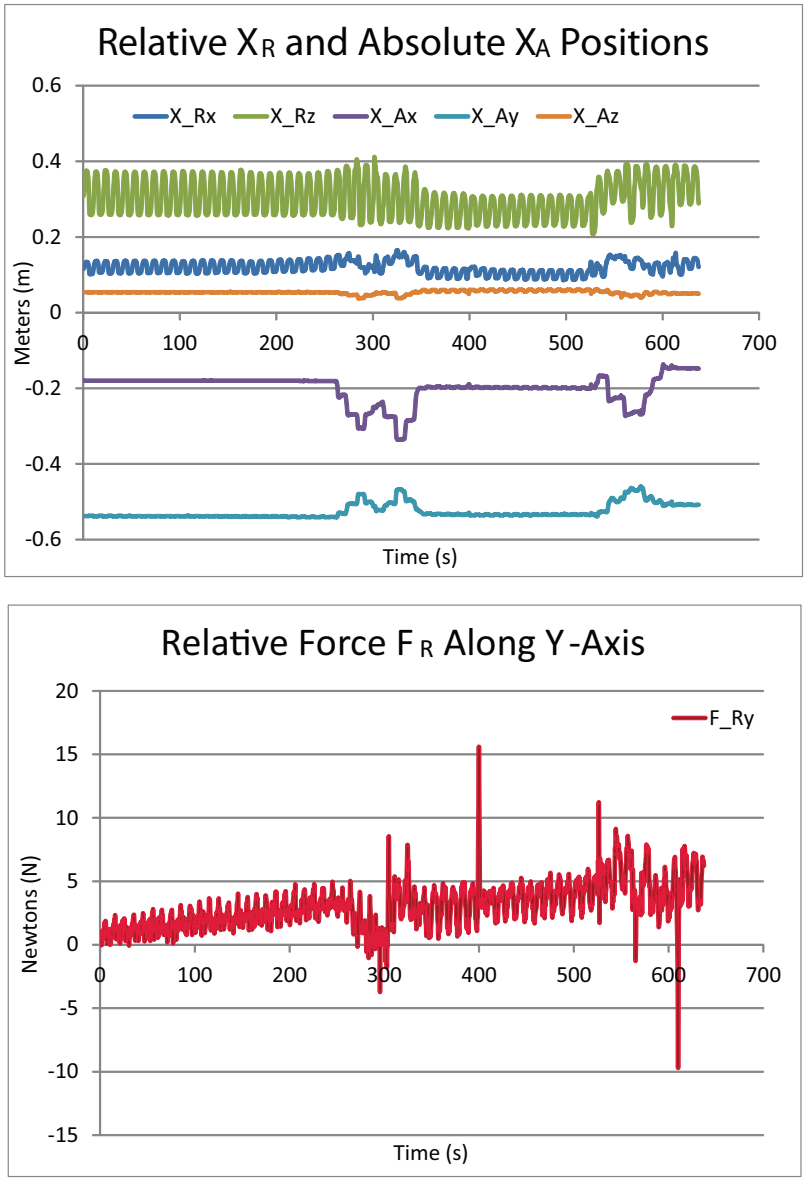

Figure 5: The graph shows the experimental data during a chain-cleaning task when the gripper (reference) arm end-effector position and null space posture were dynamically changed. Shown are the relative position components x_{Rx}, x_{Rz} and relative force f_{Ry} at the tool end-effector with respect to the gripper end-effector, as well as the absolute position of the reference end-effector x_{Ax}, x_{Ay}, x_{Az}.

up and down. The robot response is shown in Fig. 4. And lastly, in horizontal photo strip 5, the reference end-effector is moved horizontally and vertically, while the null space posture

of the reference arm is dynamically changed. The response of the robot is shown in Fig. 5. In both Figs. 4 and 5, the desired force is maintained on the average of around 5 N.

5.5. Experiment 2: The Effect of the Wrench Transformation Matrix

This second experiment will show the effect of the wrench transformation matrix ${}^2\Psi_3$ on $\mathbf{J}_R$. In previous expressions of modular relative Jacobian [36–38], the wrench transformation matrix was considered to be an identity matrix. Here, we refer to such relative Jacobian as $\mathbf{J}'_R$. The dual-arm robot will perform a coordinated independent task with respect to their relative reference frames. This is shown in Fig 6.

In this experiment robot B is to open and close a cabinet door, while robot A exerts a normal force on the other cabinet door and moving in an oscillatory manner. Force is exerted by the tool end-effector along x_{R_y}-axis. A desired sinusoidal motion along the relative $x_{R_{dz}}$-axis for the tool end-effector is specified as

$$x_{R_{dz}} = A(\cos(\omega t) - \cos(\omega t - \phi)) \tag{28}$$

where $A = 0.5\ m$ is the desired amplitude, $\omega = 0.15\pi$ rad$/s$ is the desired angular frequency, t is current time, and $\phi = 10$ degrees is the desired phase shift, which determines the magnitude of the incremental step size. The remaining relative axes are in motion control, specified to maintain the initial position and orientation. Proportional position gains are set at 200 while proportional orientation gains are at 100. Proportional force gain is set at 0.2.

Compared to Experiment 1, the Experiment 2 relative position gains can be set higher because the relative orientation of the tool end-effector is now controlled. However, the relative force gain is set at the same value as the previous experiment. The amplitude A is set higher because the tool robot now can move on a much larger surface of the cabinet door. The period ω is set lower in order to maintain an almost the same speed as the previous experiment. The offset ϕ of 10 degrees is set in order to allow incremental sinusoidal motion and thus allowing an arbitrary starting location of the oscillatory motion of the the tool end-effector.

In Experiment 2 both end-effectors perform different jobs: reference end-effector is opening and closing a cabinet door, while the tool end-effector is "polishing" the surface of the other door. The reference end-effector can be thought of as moving in an independent manner (independent from the task of the tool end-effector) while the tool end-effector moves with respect to the reference end-effector. However, the motion of the reference end-effector does not have much effect on the motion of the tool end-effector because the opening and closing of the door moves along the x_{R_y}, which is the force control direction of the tool end-effector. Thus in this manner, the tasks of both end-effectors can be considered to be independent of each other. Although the tasks are independent of each other, the

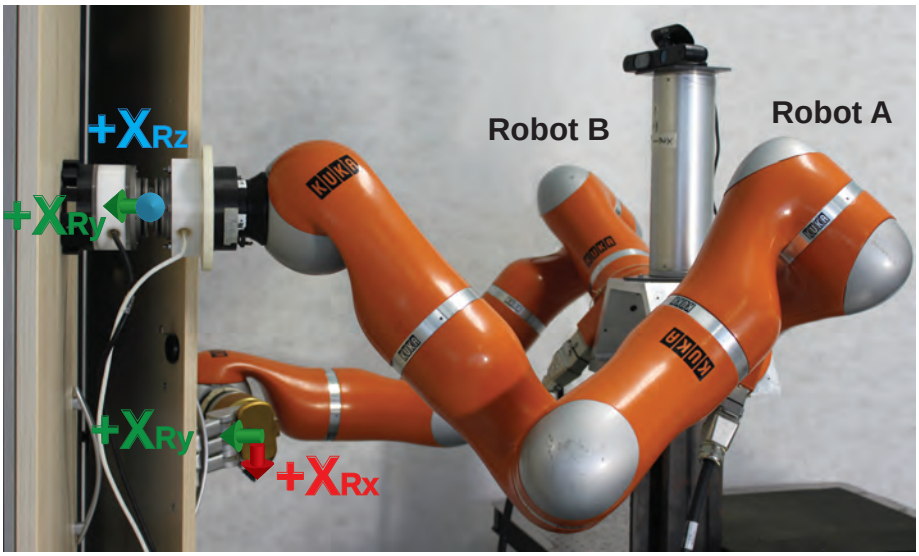

Figure 6: The KUKA dual-arm manipulator performing a coordinated independent task: robot B opening and closing a cabinet door by moving along the x_{R_y}-axis, and robot A exerting a normal force along x_{R_y}-axis on the other cabinet door while moving along an oscillatory motion along x_{R_z}-axis.

role of the unified Jacobian remains the same: it affords drastic increase in the null-space dimension and allows no restriction on the absolute locations of the task performance, because the tasks are performed in the relative reference frame. Thus, the base of the dual-arm can be anywhere with respect to the cabinet doors, but the coordinated independent tasks can still be performed. Intuitively, this means that the dual-arm base can avoid obstacles in a dynamically changing environment while the independent tasks of the two arms are performed in real-time.

The normal force feedback in shown in Fig. 7 and its corresponding position error is shown in Fig. 8. Because KUKA does not allow access to a low-level, real-time controller and the sampling frequency is at 125 Hz, the force control is expected to be non-optimal. To keep the tool end-effector to maintain contact during task execution, we specify a desired normal force of -30 N. For case $\mathbf{J}_R$, it is able to exert a normal force in the average range of around $[0,-11]$ N (Fig. 7A), while case $\mathbf{J}'_R$ is within the average range of around $[2,-5]$ N (Fig. 7B) and losing surface contact. As seen in these results, with a much more complicated task execution between the end-effectors, a much more superior force control response was shown by $\mathbf{J}_R$, exerting around double the maximum force compared to $\mathbf{J}'_R$. At the same time, the latter case consistently loses contact as indicated by an offset non-contact force of around 2 N. This offset force value was set just before task execution.

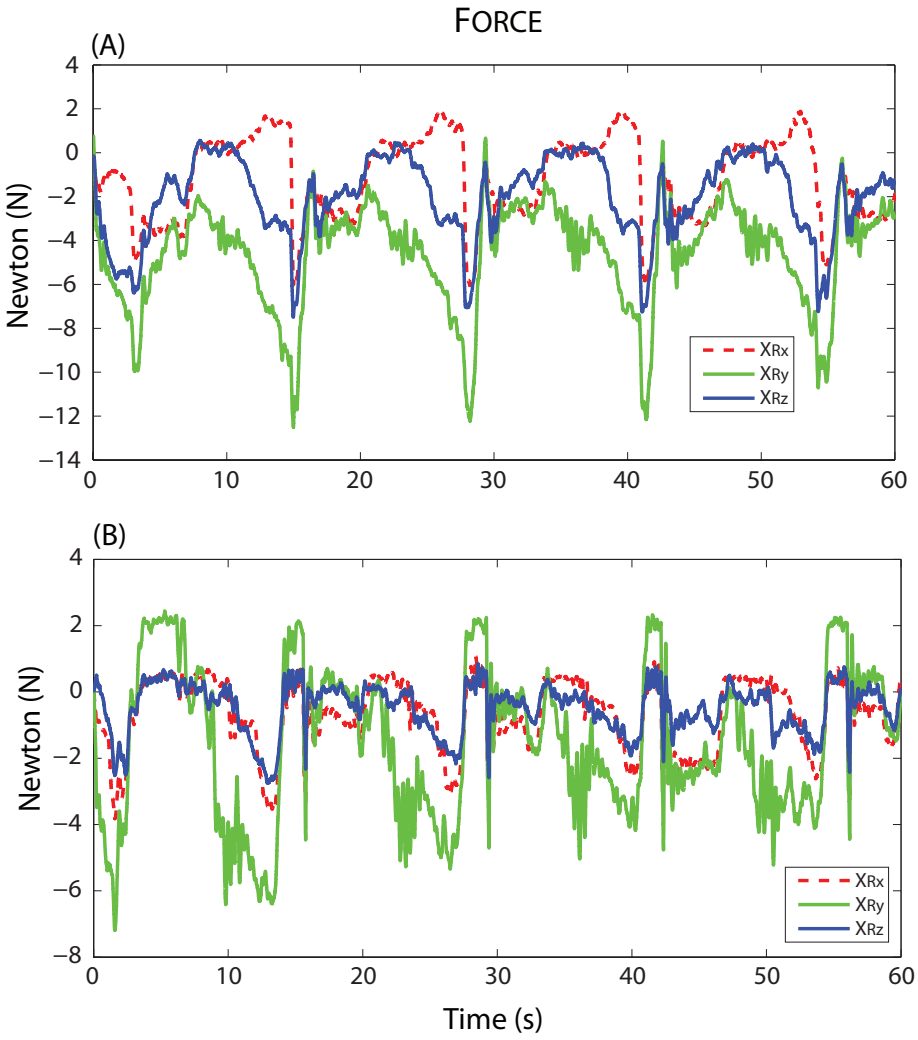

Figure 7: Force sensor feedback expressed with respect to the reference end-effector frame for the coordinated independent tasks experiment. The normal force exerted on the other cabinet door is along $\mathbf{x}_{R_y}$. Case $\mathbf{J}_R$ is shown in subfigure A and case $\mathbf{J}'_R$ is shown in subfigure B.

6. Conclusion

This work has shown a modular task-space dynamics formulation for dual arms controlled as one manipulator with a single end-effector. The aim of such an approach is the ease of implementation, by using the existing kinematics and dynamics model of each of the stand-alone manipulators to arrive at the overall dynamics of the single end-effector dual-arm. Thus, when two arms with known Jacobians and dynamics parameters are

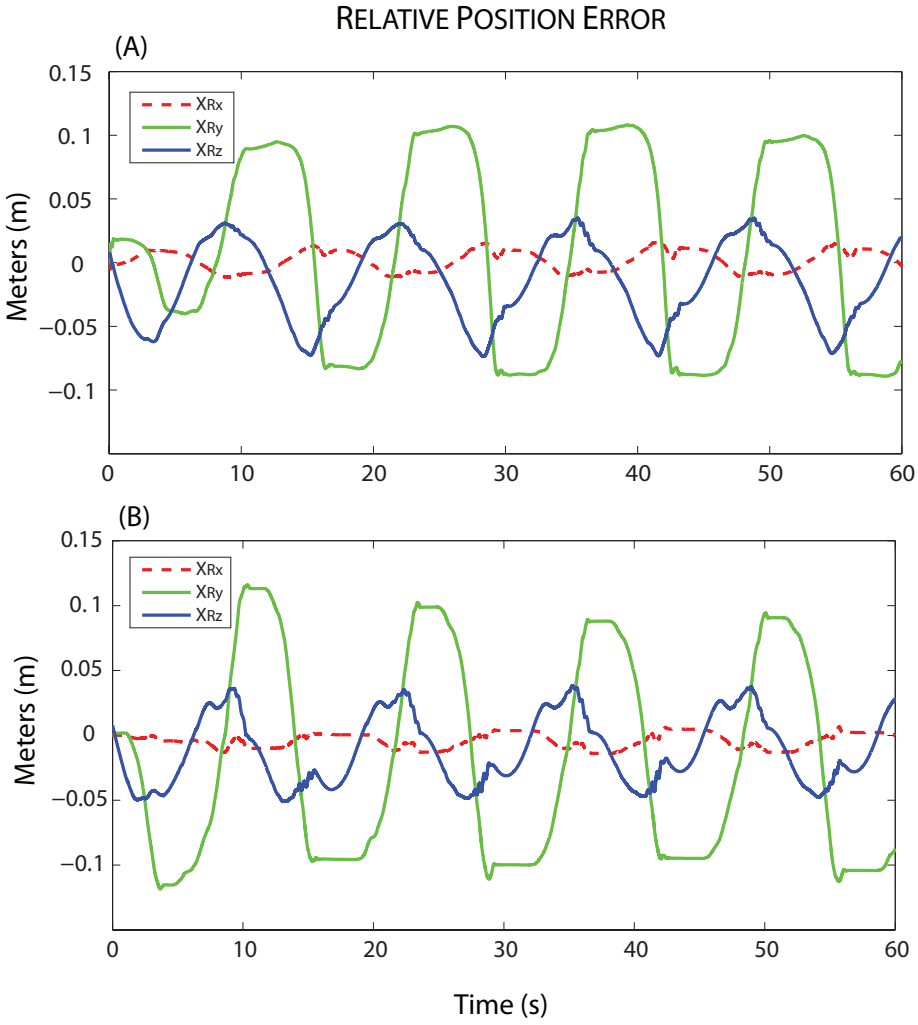

Figure 8: Relative position errors between tool end-effector and reference end-effector during coordinated independent tasks experiment. The $\mathbf{J}_R$ case is shown in subfigure A, while $\mathbf{J}'_R$ case is shown in subfigure B.

combined together, our proposed method will not require to compute and identify new dynamics for the combined system, but will use the existing information from each of the standalone components. A derivation of the modular relative task space inertia matrix is shown, together with a non-modular derivation that was used to verify the non-coupling effect of the total joint-space inertia of the dual-arm. Two experimental results are shown using a KUKA dual-arm robot: one performing a chain-cleaning task and another performing a coordinated independent task. Experiments showed superior force control performance of a dual-arm robot when the wrench transformation matrix is considered in the

modular relative Jacobian.

Acknowledgement

The authors would like to thank Roy Featherstone, Seyed Reza Ahmadzadeh and Jinoh Lee for their inputs in the development of this manuscript.

Appendix A. Non-modular Derivation of the Total Joint-Space Inertia

This section will verify the non-coupling effect of the total joint space inertia of the dual-arm, $\mathbf{A}_T$, shown in (12), by using the method of joint-space inertia derivation of a single manipulator.

Given that frame $\{i-1\}$ is located at the joint of link i and frame $\{i\}$ is at the tip, such that link i moves with respect to the z-axis of the $\{i-1\}$ frame. Further given that the i-th inertia tensor, $\mathbf{I}_i$, is expressed at frame $\{i\}$. The kinetic energy of link i can be expressed as [39],

$$KE_i = \frac{1}{2}\,\dot{\mathbf{q}}^T\,\mathbf{J}_i^T \begin{bmatrix} m_i\,\mathbf{I} & \mathbf{0} \\ \mathbf{0} & \mathbf{R}_i\,\mathbf{I}_i\,\mathbf{R}_i^T \end{bmatrix} \mathbf{J}_i\,\dot{\mathbf{q}}_i \tag{A.1}$$

where link i Jacobian, $\mathbf{J}_i$, is the manipulator Jacobian $\mathbf{J} \in \mathbb{R}^{m\times n}$ with zeros from column $i+1$ to n, that is,

$$\mathbf{J}_i = \begin{bmatrix} \mathbf{j}_1^{(1)} & \dots & \mathbf{j}_i^{(i)} & \mathbf{0}^{(i+1)} & \dots & \mathbf{0}^{(n)} \end{bmatrix}, \tag{A.2}$$

where the column indices are shown as superscripts. The symbol $\mathbf{I}$ is the corresponding identity matrix, and $\mathbf{R}_i$ is the rotation matrix corresponding to the rotation of frame $\{i\}$ with respect to the base frame of the robot. This means that the task space inertia matrix of link i, Λ_i, which is expressed as

$$\Lambda_i = \begin{bmatrix} m_i\,\mathbf{I} & \mathbf{0} \\ \mathbf{0} & \mathbf{R}_i\,\mathbf{I}_i\,\mathbf{R}_i^T \end{bmatrix} \tag{A.3}$$

can be perturbed only by joints 1 to i and not by joints $i+1$ to n. The joint space inertia matrix, $\mathbf{A}$, can be expressed as [39],

$$\mathbf{A} = \sum_{i=1}^{n} \mathbf{J}_i^T\,\Lambda_i\,\mathbf{J}_i. \tag{A.4}$$

Thus given robot A with manipulator Jacobian $\mathbf{J}_A \in \mathbb{R}^{m\times n_A}$, link j Jacobian $\mathbf{J}_{Aj}$, and link j task space inertia matrix Λ_{Aj}, the robot A joint space inertia, $\mathbf{A}_A$, can be expressed as

$$\mathbf{A}_A = \sum_{j=1}^{n_A} \mathbf{J}_{Aj}^T\,\Lambda_{Aj}\,\mathbf{J}_{Aj}. \tag{A.5}$$

In the same way, given robot B with manipulator Jacobian $\mathbf{J}_B \in \mathbb{R}^{m \times n_B}$, link k Jacobian $\mathbf{J}_{Bk}$, and link k task space inertia matrix Λ_{Bk}, the robot B joint space inertia, $\mathbf{A}_B$, can be expressed as

$$\mathbf{A}_B = \sum_{k=1}^{n_B} \mathbf{J}_{Bk}^T \Lambda_{Bk} \mathbf{J}_{Bk}. \tag{A.6}$$

By following the same analogy, the joint space inertia of the dual-arm robot, $\mathbf{A}_T$, can be computed. Given the dual-arm relative Jacobian, $\mathbf{J}_R \in \mathbb{R}^{m \times (n_A + n_B)}$, the dual-arm link i Jacobian, $\mathbf{J}_{Ri}$, can be expressed as in (A.7)

$$\begin{aligned}
\mathbf{J}_{Ri} &= \begin{cases} \begin{bmatrix} \mathbf{j}_{R1}^{(1)} & \dots & \mathbf{j}_{Ri}^{(i)} & \mathbf{0}^{(i+1)} & \dots & \mathbf{0}^{(n_A+n_B)} \end{bmatrix} & \text{for} \quad i \le n_A \\ \begin{bmatrix} \mathbf{0}^{(1)} & \dots & \mathbf{0}^{(n_A)} & \mathbf{j}_{R(n_A+1)}^{(n_A+1)} & \dots & \mathbf{j}_{Ri}^{(i)} & \mathbf{0}^{(i+1)} & \dots & \mathbf{0}^{(n_A+n_B)} \end{bmatrix} & \text{for} \quad i > n_A \end{cases} \\
&= \begin{cases} \mathbf{Q}_A \Big[\underbrace{\mathbf{j}_{A1}^{(1)} \quad \dots \quad \mathbf{j}_{Aj}^{(i)} \quad \mathbf{0}^{(i+1)} \quad \dots \quad \mathbf{0}^{(n_A)}}_{\mathbf{J}_{Aj}} \quad \mathbf{0}^{(n_A+1)} \quad \dots \quad \mathbf{0}^{(n_A+n_B)} \Big] & \text{for} \quad i \le n_A \\ \mathbf{Q}_B \Big[\mathbf{0}^{(1)} \quad \dots \quad \mathbf{0}^{(n_A)} \quad \underbrace{\mathbf{j}_{B1}^{(n_A+1)} \quad \dots \quad \mathbf{j}_{Bk}^{(i)} \quad \mathbf{0}^{(i+1)} \quad \dots \quad \mathbf{0}^{(n_A+n_B)}}_{\mathbf{J}_{Bk}} \Big] & \text{for} \quad i > n_A \end{cases}
\end{aligned} \tag{A.7}$$

where $i = 1, \dots, n_A + n_B$, $j = 1, \dots, n_A$, and $k = 1, \dots, n_B$. In the second equality of (A.7), for the case of $i \le n_A$, columns 1 to n_A represent $\mathbf{J}_{Aj}$. For the case of $i > n_A$, columns $(n_A + 1)$ to $(n_A + n_B)$ represent $\mathbf{J}_{Bk}$. This means that in accounting for the kinetic energy generated by the motion of link i of the dual-arm robot, this link i can only be perturbed by either robot A or robot B, and not both. From (A.4), we set $n = n_A + n_B$ such that the sum of all the joint space inertias of the dual-arm is

$$\begin{aligned}
\mathbf{A}_T &= \sum_{i=1}^{n_A} \mathbf{J}_{Ri}^T \Lambda_{Ai} \mathbf{J}_{Ri} + \sum_{i=n_A+1}^{n_A+n_B} \mathbf{J}_{Ri}^T \Lambda_{B(i-n_A)} \mathbf{J}_{Ri} \\
&= \sum_{j=1}^{n_A} \begin{bmatrix} \mathbf{J}_{Aj}^T \\ \mathbf{0}^T \end{bmatrix} \mathbf{Q}_A^T \Lambda_{Aj} \mathbf{Q}_A \begin{bmatrix} \mathbf{J}_{Aj} & \mathbf{0} \end{bmatrix} + \sum_{k=1}^{n_B} \begin{bmatrix} \mathbf{0}^T \\ \mathbf{J}_{Bk}^T \end{bmatrix} \mathbf{Q}_B^T \Lambda_{Bk} \mathbf{Q}_B \begin{bmatrix} \mathbf{0} & \mathbf{J}_{Bk} \end{bmatrix} \\
&= \begin{bmatrix} \sum_{j=1}^{n_A} \mathbf{J}_{Aj}^T \mathbf{Q}_A^T \Lambda_{Aj} \mathbf{Q}_A \mathbf{J}_{Aj} & \mathbf{0} \\ \mathbf{0} & \sum_{k=1}^{n_B} \mathbf{J}_{Bk}^T \mathbf{Q}_B^T \Lambda_{Bk} \mathbf{Q}_B \mathbf{J}_{Bk} \end{bmatrix}
\end{aligned} \tag{A.8}$$

From the last equality above, we can see that the diagonal terms are equivalent to (A.5) and (A.6). The existence of $\mathbf{Q}_A$ and $\mathbf{Q}_B$ in the expression takes care of the fact that the link inertias are expressed at the relative task-space before converting to joint-space inertias. However, this derivation upholds the non-coupling of the total joint-space inertia of the dual-arm.

References

References

[1] N. G. Tsagarakis, S. Morfey, G. M. Cerda, L. Zhibin, and D. G. Caldwell, "Compliant humanoid coman: Optimal joint stiffness tuning for modal frequency control," in *Robotics and Automation (ICRA), 2013 IEEE International Conference on*. IEEE, 2013, pp. 673–678.

[2] M. Hirose and K. Ogawa, "Honda humanoid robots development," *Philosophical Transactions of the Royal Society A: Mathematical, Physical and Engineering Sciences*, vol. 365, no. 1850, pp. 11–19, 2007.

[3] G. Metta, L. Natale, F. Nori, G. Sandini, D. Vernon, L. Fadiga, C. Von Hofsten, K. Rosander, M. Lopes, J. Santos-Victor, *et al.*, "The iCub humanoid robot: An open-systems platform for research in cognitive development," *Neural Networks*, vol. 23, no. 8, pp. 1125–1134, 2010.

[4] C. Borst, C. Ott, T. Wimbock, B. Brunner, F. Zacharias, B. Bauml, U. Hillenbrand, S. Haddadin, A. Albu-Schaffer, and G. Hirzinger, "A humanoid upper body system for two-handed manipulation," in *Robotics and Automation (ICRA), 2007 IEEE International Conference on*. IEEE, 2007, pp. 2766–2767.

[5] A. Dietrich, T. Wimbock, A. Albu-Schaffer, and G. Hirzinger, "Reactive whole-body control: Dynamic mobile manipulation using a large number of actuated degrees of freedom," *Robotics & Automation Magazine, IEEE*, vol. 19, no. 2, pp. 20–33, 2012.

[6] O. Khatib, "Inertial properties in robotic manipulation: An object-level framework," *The International Journal of Robotics Research*, vol. 14, no. 1, pp. 19–36, 1995.

[7] M. Vukobratovic, V. Potkonjak, and S. Tzafestas, "Human and humanoid dynamics," *Journal of Intelligent and Robotic Systems*, vol. 41, no. 1, 2004.

[8] S. Hyon, J. G. Hale, and G. Cheng, "Full-body compliant human–humanoid interaction: balancing in the presence of unknown external forces," *Robotics, IEEE Transactions on*, vol. 23, no. 5, pp. 884–898, 2007.

[9] O. Khatib, L. Sentis, and J.-H. Park, "A unified framework for whole-body humanoid robot control with multiple constraints and contacts," in *European Robotics Symposium 2008*. Springer, 2008, pp. 303–312.

[10] T. Reichenbach, "A dynamic simulator for humanoid robots," *Artificial Life and Robotics*, vol. 13, no. 2, pp. 561–565, 2009.

[11] H. Dallali, M. Mosadeghzad, G. A. Medrano-Cerda, N. Docquier, P. Kormushev, N. Tsagarakis, Z. Li, and D. Caldwell, "Development of a dynamic simulator for a compliant humanoid robot based on a symbolic multibody approach," in *Mechatronics (ICM), 2013 IEEE International Conference on*. IEEE, 2013, pp. 598–603.

[12] B. J. Stephens and C. G. Atkeson, "Dynamic balance force control for compliant humanoid robots," in *Intelligent Robots and Systems (IROS), 2010 IEEE/RSJ International Conference on*. IEEE, 2010, pp. 1248–1255.

[13] C. Ott, A. Dietrich, and M. A. Roa, "Torque-based multi-task and balancing control for humanoid robots," in *Ubiquitous Robots and Ambient Intelligence (URAI), 2014 11th International Conference on*. IEEE, 2014, pp. 143–144.

[14] A. Konno, T. Myojin, T. Matsumoto, T. Tsujita, and M. Uchiyama, "An impact dynamics model and sequential optimization to generate impact motions for a humanoid robot," *The International Journal of Robotics Research*, vol. 30, no. 13, pp. 1596–1608, 2011.

[15] V. Potkonjak, S. Tzafestas, M. Vukobratovic, M. Milojevic, and M. Jovanovic, "Human-and-humanoid postures under external disturbances: Modeling, simulation, and robustness. part 1: Modeling," *Journal of Intelligent & Robotic Systems*, vol. 63, no. 2, pp. 191–210, 2011.

[16] D. E. Orin, A. Goswami, and S.-H. Lee, "Centroidal dynamics of a humanoid robot," *Autonomous Robots*, vol. 35, no. 2-3, pp. 161–176, 2013.

[17] O. E. R. Ponce, "Generation of the whole-body motion for humanoid robots with the complete dynamics," Ph.D. dissertation, Universite Toulouse III Paul Sabatier, 2014.

[18] N. Paine, J. S. Mehling, J. Holley, N. A. Radford, G. Johnson, C.-L. Fok, and L. Sentis, "Actuator control for the nasa-jsc valkyrie humanoid robot: A decoupled dynamics approach for torque control of series elastic robots," *Journal of Field Robotics*, vol. 32, no. 3, pp. 378–396, 2015.

[19] S. Liu, L. Wu, and Z. Lu, "Impact dynamics and control of a flexible dual-arm space robot capturing an object," *Applied Mathematics and Computation*, vol. 185, no. 2, pp. 1149–1159, 2007.

[20] F. Caccavale, P. Chiacchio, A. Marino, and L. Villani, "Six-dof impedance control of dual-arm cooperative manipulators," *Mechatronics, IEEE/ASME Transactions on*, vol. 13, no. 5, pp. 576–586, 2008.

[21] Y.-s. Guo and L. Chen, "Adaptive neural network control for coordinated motion of a dual-arm space robot system with uncertain parameters," *Applied Mathematics and Mechanics*, vol. 29, pp. 1131–1140, 2008.

[22] W. Xu, Y. Liu, and Y. Xu, "The coordinated motion planning of a dual-arm space robot for target capturing," *Robotica*, vol. 30, no. 05, pp. 755–771, 2012.

[23] N. Yagiz, Y. Hacioglu, and Y. Z. Arslan, "Load transportation by dual arm robot using sliding mode control," *Journal of Mechanical Science and Technology*, vol. 24, no. 5, pp. 1177–1184, 2010.

[24] Y. Hacioglu, Y. Z. Arslan, and N. Yagiz, "Mimo fuzzy sliding mode controlled dual arm robot in load transportation," *Journal of the Franklin Institute*, vol. 348, no. 8, pp. 1886–1902, 2011.

[25] T. Wimböck and C. Ott, "Dual-arm manipulation," in *Towards Service Robots for Everyday Environments*. Springer, 2012, pp. 353–366.

[26] A. Tavasoli, M. Eghtesad, and H. Jafarian, "Two-time scale control and observer design for trajectory tracking of two cooperating robot manipulators moving a flexible beam," *Robotics and Autonomous Systems*, vol. 57, no. 2, pp. 212–221, 2009.

[27] C. Lewis and A. Maciejewski, "Trajectory generation for cooperating robots," in *Systems Engineering, 1990 IEEE International Conference on*. IEEE, 1990, pp. 300–303.

[28] C. Lewis, "Trajectory generation for two robots cooperating to perform a task," in *Robotics and Automation (ICRA), 1996 IEEE International Conference on*, vol. 2. IEEE, 1996, pp. 1626–1631.

[29] R. S. Jamisola and R. G. Roberts, "A more compact expression of relative jacobian based on individual manipulator jacobians," *Robotics and Autonomous Systems*, no. Part 1, pp. 158–164, 2015.

[30] O. Khatib, "A unified approach for motion and force control of robot manipulators: The operational space formulation," *Robotics and Automation, IEEE Journal of*, vol. 3, no. 1, pp. 43–53, 1987.

[31] R. Jamisola, M. H. Ang Jr, D. Oetomo, O. Khatib, T. M. Lim, and S. Y. Lim, "The operational space formulation implementation to aircraft canopy polishing using a mobile manipulator," in *Robotics and Automation (ICRA), 2002 IEEE International Conference on*, vol. 1. IEEE, 2002, pp. 400–405.

[32] R. S. Jamisola, D. N. Oetomo, M. H. Ang, O. Khatib, T. M. Lim, and S. Y. Lim, "Compliant motion using a mobile manipulator: an operational space formulation approach to aircraft canopy polishing," *Advanced Robotics*, vol. 19, no. 5, pp. 613–634, 2005.

[33] R. Jamisola, M. Ang Jr, T. M. Lim, O. Khatib, and S. Y. Lim, "Dynamics identification and control of an industrial robot," in *Advanced Robotics (ICAR), 1999 9th Internaional Conference on*, 1999, pp. 323–328.

[34] R. Jamisola, "Full dynamics identification and control of PUMA 560 and Mitsubishi PA-10 robots," Master's thesis, Masters thesis, National University of Singapore, Department of Mechanical and Production Engineering, 2001.

[35] R. S. Jamisola Jr and E. P. Dadios, "Experimental identification of manipulator dynamics through the minimization of its natural oscillations," *Journal of Advanced Computational Intelligence and Intelligent Informatics*, vol. 14, no. 1, pp. 39–45, 2010.

[36] P. Chiacchio, S. Chiaverini, and B. Siciliano, "Task-oriented kinematic control of two cooperative 6-dof manipulators," in *American Control Conference, 1993*. IEEE, 1993, pp. 336–340.

[37] B. Cao, G. I. Dodds, and G. W. Irwin, "Redundancy resolution and obstacle avoidance for cooperative industrial robots," *Journal of Robotic Systems*, vol. 16, no. 7, pp. 405–417, 1999.

[38] J. Lee, P. H. Chang, and R. Jamisola, "Relative impedance control for dual-arm robots performing asymmetric bimanual tasks," *Industrial Electronics, IEEE Transactions on*, vol. 61, no. 7, pp. 3786–3796, July 2014.

[39] L. Sciavicco and B. Siciliano, *Modelling and control of robot manipulators*. Springer, 2000.